

On the binary nature of the γ -ray sources AGL J2241+4454 (=MWC 656) and HESS J0632+057 (=MWC 148)

J. Casares^{1,2*}, M. Ribó³, I. Ribas⁴, J.M. Paredes³, F. Vilardell⁵, I. Negueruela⁵

¹ *Instituto de Astrofísica de Canarias, E-38200 La Laguna, Tenerife, Spain*

² *Departamento de Astrofísica, Universidad de La Laguna, Avda. Astrofísico Francisco Sánchez s/n, E-38271 La Laguna, Tenerife, Spain*

³ *Departament d'Astronomia i Meteorologia, Institut de Ciències del Cosmos (ICC), Universitat de Barcelona (IEEC-UB), Martí i Franquès 1, E-08028 Barcelona, Spain*

⁴ *Institut de Ciències de l'Espai – (IEEC-CSIC), Campus UAB, Facultat de Ciències, Torre C5 - parell - 2a planta, E-08193 Bellaterra, Spain*

⁵ *Departamento de Física, Ingeniería de Sistemas y Teoría de la Señal, Universidad de Alicante, Apdo. 99, E-03080 Alicante, Spain*

13 October 2018

ABSTRACT

We present optical spectroscopy of MWC 656 and MWC 148, the proposed optical counterparts of the γ -ray sources AGL J2241+4454 and HESS J0632+057, respectively. The main parameters of the $H\alpha$ emission line (EW , $FWHM$ and centroid velocity) in these stars are modulated on the proposed orbital periods of 60.37 and 321 days, respectively. These modulations are likely produced by the resonant interaction of the Be discs with compact stars in eccentric orbits. We also present radial velocity curves of the optical stars folded on the above periods and obtain the first orbital elements of the two γ -ray sources thus confirming their binary nature. Our orbital solution support eccentricities $e \sim 0.4$ and 0.83 ± 0.08 for MWC 656 and MWC 148, respectively. Further, our orbital elements imply that the X-ray outbursts in HESS J0632+057/MWC 148 are delayed ~ 0.3 orbital phases after periastron passage, similarly to the case of LS I +61 303. In addition, the optical photometric light curve maxima in AGL J2241+4454/MWC 656 occur ~ 0.25 phases passed periastron, similar to what is seen in LS I +61 303. We also find that the orbital eccentricity is correlated with orbital period for the known γ -ray binaries. This is explained by the fact that small stellar separations are required for the efficient triggering of VHE radiation. Another correlation between the EW of $H\alpha$ and orbital period is also observed, similarly to the case of Be/X-ray binaries. These correlations are useful to provide estimates of the key orbital parameters P_{orb} and e from the $H\alpha$ line in future Be γ -ray binary candidates.

Key words: stars:emission-line, Be – stars: individual: MWC 656 – stars: individual: MWC 148 – gamma rays: stars – X-rays: stars.

1 INTRODUCTION

Cherenkov telescopes are opening a new era of discoveries with the detection of large populations of γ -ray sources ranging from galactic objects (supernovae remnants, pulsar-wind nebulae, compact binaries) to distant blazars and starburst galaxies (Hinton & Hofmann 2009). In particular, the class of γ -ray binaries has attracted great attention in the last few

years. They are characterised by the presence of a compact star orbiting a late-O/early B companion. Either if particles are accelerated in a microquasar jet or in the collision of two winds, the high density of UV photons from the massive star provides the necessary environment for the production of GeV-TeV emission through inverse Compton scattering. There are currently three confirmed γ -ray binaries with High Energy (HE, $E > 100$ MeV) and/or Very High Energy (VHE, $E > 100$ GeV) emission modulated on the orbital period: PSR B1259–63, LS 5039 and LS I +61 303 (Paredes 2011). Three more candidates have been recently proposed but their binary nature awaits confirmation. These are 1FGL

* E-mail: jorge.casares@iac.es (JCV); mribo@am.ub.es (MR); iribas@ieec.uab.es (IR); jmparedes@ub.edu (JMP); vilardell@ice.cat (FV); ignacio@dfists.ua.es (IN)

J1018.6–5856 (Corbet et al. 2011), AGL J2241+4454 and HESS J0632+057. The latter two sources are the subject of this paper.

AGL J2241+4454 is a point-like γ -ray source detected by the AGILE satellite above 100 MeV (Lucarelli et al. 2010). The error circle of the satellite contains the Be star MWC 656 (= HD 215227) which was proposed by Williams et al. (2010) as the likely optical counterpart. The same authors suggest a spectral classification B3 IVne+sh and an orbital period of 60.37 ± 0.04 d based on Hipparcos light curve data. By fitting the spectral energy distribution in the UV and *B*-band a distance of 2.6 ± 1.0 kpc is derived. This, combined with its high Galactic latitude $b = -12^\circ$, implies a runaway star, another evidence supporting its binary nature.

On the other hand, MWC 148 (=HD 259440) is a B0 Vpe star which has been proposed as the optical counterpart of the TeV source HESS J0632+057 (Aharonian et al. 2007). The claim is based on the detection of radio (Skilton et al. 2009) and X-ray emission associated to MWC 148 (Hinton et al. 2009; Falcone et al. 2010) with similar spectral indexes and variability as observed in PSR B1259–63, LS 5039 and LS I +61 303. Recently, extended and variable radio emission at AU scales, showing similar morphology to these three γ -ray binaries, has been reported (Moldón et al. 2011a; see also Moldón et al. 2011b, Ribó et al. 2008 and Dhawan et al. 2006). Lower limits to the orbital period of >54 d (Falcone et al. 2010) and >200 d (Casares et al. 2011) were proposed based on X-ray and optical emission line variability. Further, the absence of significant radial velocity shifts in the B0 star supports a long period >100 d (Aragona et al. 2010). Finally, Bongiorno et al. (2011) report the presence of strong X-ray flares in *Swift*/XRT data, modulated with a period of 321 \pm 5 d which strongly advocates for its binary nature.

Alternative scenarios to the binary hypothesis invoke an isolated star where high energy emission is produced in a wind driven shock. In particular, Bp stars are known to possess strong surface magnetic fields which efficiently confine the stellar wind and may accelerate particles up to TeV energies (Townsend et al. 2007). The best way to test the binary model and solve the system geometry is through a radial velocity study and hence we have embarked in an optical spectroscopic campaign of MWC 656 and MWC 148 using several telescopes. Our analysis demonstrates that these stars are indeed the optical companions of High Mass X-ray/ γ -ray Binaries responsible for the HE/VHE emission of AGL J2241+4454 and HESS J0632+057. In the following sections we present the observations, our best constraints to the orbital parameters and discussion of results.

2 OBSERVATIONS

2.1 MWC 656

We observed MWC 656 using the Fibre-fed RObotic Dual-beam Optical Spectrograph (FRODOspec) on the robotic 2.0m Liverpool telescope (LT) at the Observatorio del Roque de Los Muchachos between 23 April and 28 July 2011. The spectrograph is fed by a fiber bundle array consisting of 12x12 lenslets of 0.82'' each which is reformatted as a slit.

The spectrograph was operated in high resolution mode, providing a dispersion of $0.35 \text{ \AA pix}^{-1}$ and spectral resolving power $R \sim 5500$ in the blue arm while $0.80 \text{ \AA pix}^{-1}$ and $R \sim 5300$ in the red arm. The spectral coverage was 3900–5215 \AA and 5900–8000 \AA respectively. A total of thirty two 600s spectra were obtained with the blue arm and sixty four 290s spectra with the red arm. One blue and two red spectra were obtained on each observing night. A log of the observations is presented in Table 1. The FRODOspec pipeline produces fully extracted and wavelength calibrated spectra with $\text{rms} \leq 0.1 \text{ \AA}$ above 4400 \AA . The analysis presented in this paper has been performed with the FRODOspec pipeline products.

2.2 MWC 148

MWC 148 was observed with the Intermediate Dispersion Spectrograph (IDS) attached to the 2.5 m Isaac Newton Telescope (INT) at the Observatorio del Roque de Los Muchachos on the nights of 20–23 October 2008. A total of 35 spectra were obtained in the blue spectral range (3900–5500 \AA , unvignetted) using the R900V grating in combination with the 235 mm camera and a 1.2'' slit to provide a spectral resolution of 80 km s^{-1} (FWHM). Nightly averages were produced from the individual spectra resulting in a total of 3 INT spectra.

Twelve additional blue spectra were obtained on the nights of 7–8 and 10–11 December 2008 with the Intermediate Dispersion Spectrograph and Imaging System (ISIS) double-arm spectrograph on the William Herschel Telescope (WHT). Here we employed the 600B and 1200B gratings on the blue arm resulting in wavelength coverages 3800–5400 \AA and 3700–4500 \AA respectively. A 1'' slit was selected yielding spectral resolutions in the range 65–115 km s^{-1} . Meanwhile, the 600R and 1200R gratings were mounted on the ISIS red arm, centered at different wavelengths, to yield simultaneous spectra in the H α and CaII NIR triplet. Nightly averages were produced for the different spectral configurations.

The High Efficiency and Resolution Mercator Echelle Spectrograph (HERMES) on the 1.2m MERCATOR (MT) telescope was also used to obtain three nightly 1800 second spectra on the nights of 30–31 October, 1–4 and 6–8 November 2009. HERMES is a fiber-fed spectrograph and we employed the high resolution mode which yield a resolving power $R = 85000$ across the entire optical range between 3770–9000 \AA . The signal-to-noise in the HERMES spectra is significantly lower than in the INT and WHT data so we decided to co-add the three individual spectra obtained every night resulting in a total of 9 Mercator spectra.

Twenty two high-resolution echelle spectra were also obtained in the period Jan 20–Apr 8 2010 using the fiber-fed STELLA Echelle Spectrograph (SES) of the 1.2m robotic STELLA-I (ST) telescope at the Observatorio del Teide in Tenerife. The spectra cover the wavelength range 3870–8800 \AA with increasing inter-order gaps starting at 7200 \AA . The spectrograph provides an effective resolving power $R = 55000$. One spectrum was obtained per night and the exposure time was set to 1800 s.

Finally, MWC 148 was also observed with FRODOspec at the LT between 4 Sep 2010 and 3 May 2011 using the

Table 1. Log of the MWC 656 observations.

Date	Telescope	Spect. Range Å	Number of spectra	Exp. Time (seconds)	Dispersion (Å pix ⁻¹)
23 Apr – 28 Jul 2011	LT	3900–5215	32	600	0.35
23 Apr – 28 Jul 2011	LT	5900–8000	64	290	0.80

Table 2. Log of the MWC 148 observations.

Date	Telescope	Spect. Range Å	Number of spectra	Exp. Time (seconds)	Dispersion (Å pix ⁻¹)
20 Oct 2008	INT	3900–5500	10	90	0.63
21 Oct 2008	INT	3900–5500	5	90	0.63
22 Oct 2008	INT	3900–5500	10,10	120,90	0.63
07 Dec 2008	WHT	3800–5400	3	20	0.88
07 Dec 2008	WHT	8300–8960	3	20	0.99
08 Dec 2008	WHT	3800–5400	3	20	0.88
08 Dec 2008	WHT	5555–7070	3	20	0.99
10 Dec 2008	WHT	3700–4500	3	25	0.45
10 Dec 2008	WHT	8335–9075	3	15	0.48
11 Dec 2008	WHT	3700–4500	3	25	0.45
11 Dec 2008	WHT	8335–9075	3	15	0.48
30 Oct-8 Nov 2009	MT	3770–9000	27	1800	0.02
20 Jan-8 Apr 2010	ST	3870–8800	22	1800	0.10
4 Sep 2010-3 May 2011	LT	3900–5215	40	600	0.35
4 Sep 2010-20 Oct 2010	LT	5900–8000	48	193	0.80
24 Oct 2010-3 May 2011	LT	5900–8000	47	290	0.80

same configuration as for MWC 656 (see above). One 600s spectrum and two 290 s or three 193 s red spectra were obtained per night. A full log of the observations is presented in Table 2.

The INT, WHT and MT spectra were reduced using standard techniques including debiasing and flatfielding. The spectra were subsequently extracted using optimal extraction techniques in order to optimize the signal-to-noise ratio of the output (Horne 1986). Frequent observations of comparison arc lamp or hollow cathode lamp images were performed in the course of each run and the pixel-to-wavelength scale was derived through polynomial fits to a large number of identified reference lines. The final rms scatter of the fit was always $<1/30$ of the spectral dispersion. The automatic pipeline products were used for the ST and the LT data.

The spectral type standard HR 2479 (B0 III) was also observed with all different telescopes and instrument configurations for the purpose of computing the rotational broadening of the companion star. It was selected because of its low projected rotational velocity of 50 km s^{-1} (Abt et al. 2002).

3 DESCRIPTION OF THE SPECTRA AND ROTATIONAL BROADENING

All the spectra were rectified by dividing a low order spline fit to the continuum. For comparison, Figure 1 displays the averaged normalised LT spectra of MWC 148 and MWC 656. Both targets show similar spectra, with very broad and shallow photospheric absorption lines. Strong Balmer emission is seen out to $H\beta$ in MWC 656 and to $H\gamma$ in MWC 148. The $H\beta$ line shows a double-peaked profile characteristic of circumstellar discs. Several Fe II disc emission lines are also detected. In summary, both spectra are typical of early-type

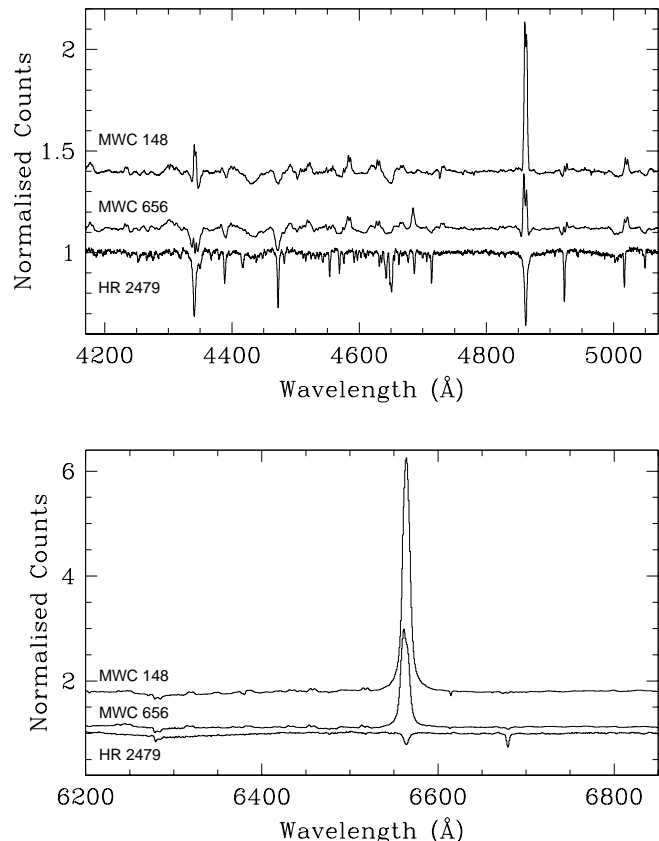


Figure 1. Average LT spectra of MWC 148 and MWC 656 in the blue (top panel) and red (bottom panel) spectral regions. The bottom spectra show the B0 III star HR 2479 for comparison, which has an intrinsic broadening of 50 km s^{-1} .

Be stars with well developed discs fed by stable mass loss (Porter & Rivinius 2003). Detailed spectral analysis performed by Williams et al. (2010) and Aragona et al. (2010) support a spectral classification B3 IVne+sh for MWC 656 and B0 Vpe for MWC 148. In the remaining of this paper we have adopted the spectral classification and stellar parameters derived in these works.

Projected rotational velocities of 430 km s^{-1} (Gutiérrez-Soto et al. 2007) and 500 km s^{-1} (Aragona et al. 2010) have been reported for MWC 148 whereas $262 \pm 26 \text{ km s}^{-1}$ (Yudin 2001) and $300 \pm 50 \text{ km s}^{-1}$ (Williams et al. 2010) for MWC 656. We decided to estimate the rotational broadening $v \sin i$ from our own spectra following the technique outlined in Marsh et al. (1994), which basically subtracts broadened templates from the average spectrum of the target and searches for the lowest residual. Therefore, we first rebinned our LT spectra of the two stars and the template HR 2479 into a uniform velocity scale of 23 km s^{-1} per pixel. The template was subsequently broadened from 100 to 500 km s^{-1} in steps on 5 km s^{-1} using a Gray rotational profile (Gray 1992) with a limb darkening coefficient $\epsilon = 0.33$. The broadened versions of the template were multiplied by a scaling factor ≤ 1 to account for dilution due to extra sources of continuum light (such as the equatorial Be disc) and subtracted from the averaged spectra of the two targets. The subtraction was restricted to the blue spectral range $4400\text{--}5200 \text{ \AA}$, where the photospheric He I, He II and metallic lines are most prominent. The IS, Balmer and Fe II emission lines were all masked in the process. A χ^2 test on the residuals of the subtraction yields optimum rotational broadening of 370 km s^{-1} for MWC 148 and 342 km s^{-1} for MWC 656, with a formal uncertainty of $\pm 10 \text{ km s}^{-1}$. The rotational velocity of the template star needs to be added quadratically to these, resulting in $v \sin i = 373 \text{ km s}^{-1}$ for MWC 148 and 346 km s^{-1} for MWC 656. The same analysis was repeated for MWC 148 using the other instrument configurations and we always obtain values in the range $355\text{--}381 \text{ km s}^{-1}$.

4 ANALYSIS OF MWC 656

Be discs in X-ray binaries typically display long-term super-orbital variability associated to activity episodes, but sometimes also variability modulated with the binary orbital period (Zamanov et al. 1999). The strong H α emission is the best tracer of disc variability and hence we decided to analyse several line parameters in MWC 656 and test whether they are modulated with the claimed 60.37 d orbital period (Williams et al. 2010). First, we measured the equivalent width (EW hereafter) by integrating the H α emission profile in the 64 individual spectra. In addition, the $FWHM$ and velocity shift of the line centroid were extracted through simple Gaussian fits. The left panel of Figure 2 presents the evolution of the H α parameters with time. Because our base line extends over just 96 days we cannot probe for the presence of a 60.37 d modulation through a period search analysis.

The EW is fairly stable during our observations with a mean of $\sim 23 \text{ \AA}$ and a smooth increase toward the end of our observing window. A peak is detected at HJD 2455725 but, unfortunately, we lack the necessary time coverage to check

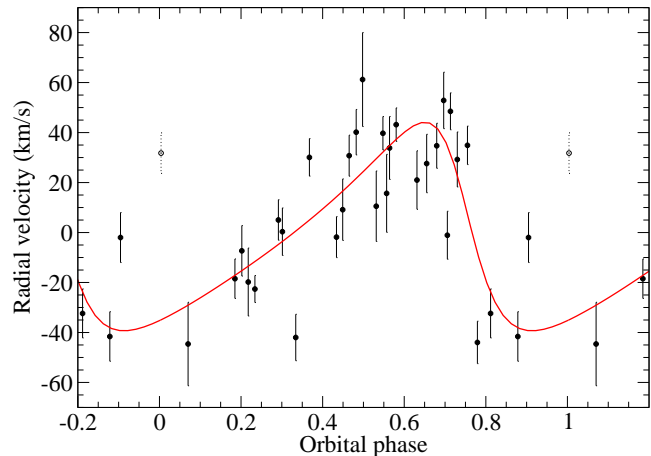


Figure 3. Radial velocity curve of MWC 656 folded on the 60.37 d period. The best-fitting solution, using an eccentric orbit with $e = 0.4$, is overplotted. The dotted point (at phase ~ 0.0) has been masked from the fit. Phase 0 is set to HJD 2453243.3.

for repeatability with a 60 d period. On the other hand, the $FWHM$ and centroid velocity do display significant variability, with two maxima elapsed by $\sim 60 \text{ d}$, in good agreement with the photometric modulation of Williams et al. (2010). The behaviour of the H α line parameters with the 60.37 d period is presented in the right panel of Figure 2.

Next, we attempted to measure radial velocities from the photospheric lines of the Be star. This is complicated by the fact that these lines are extremely broad and, in most cases, blended with disc emission lines e.g. the He I lines at 4922 \AA and 5015 \AA partly overlap with Fe II emissions at 4924 \AA and 5018 \AA (see Figure 1). After careful comparison of the average spectrum of MWC 656 with the broadened template HR 2479, we decided to restrict the radial velocity analysis to three spectral windows covering the He I lines 4471 \AA , 4713 \AA and 5048 \AA . We measured radial velocities by cross-correlating each spectrum of MWC 656 with a template formed from the average of the entire database. We find that this yields better results than using the broadened version of HR 2479 as template. The radial velocity of the template was determined by fitting a Gaussian to the core of the He I 4471 \AA line and it was added to the velocities obtained from the cross-correlation. Figure 3 presents the final radial velocities folded on the 60.37 d period of Williams et al. (2010). The plot reveals a sine-like modulation which hints for a moderate eccentricity.

The radial velocity curve was subsequently modelled with an eccentric orbital solution using the Spectroscopic Binary Orbit Program (SBOP, Etzel 1985). The orbital period was fixed to 60.37 d and phase 0 arbitrarily set to HJD 2453243.3 which corresponds to the epoch of maximum brightness in the photometric light curve (Williams et al. 2010). Individual points were weighted proportionally to $1/\sigma^2$, where σ is the radial velocity uncertainty. In the solutions we adjusted the following orbital parameters: argument of the periastron (ω), systemic velocity (γ), phase of the periastron (ϕ_{peri}) and velocity semi-amplitude (K_{opt}). The solution does not converge if the orbit eccentricity (e) is left free. Therefore, we attempted several fits fixing the eccentricity by hand and find a minimum rms for $e = 0.4$. Fitting

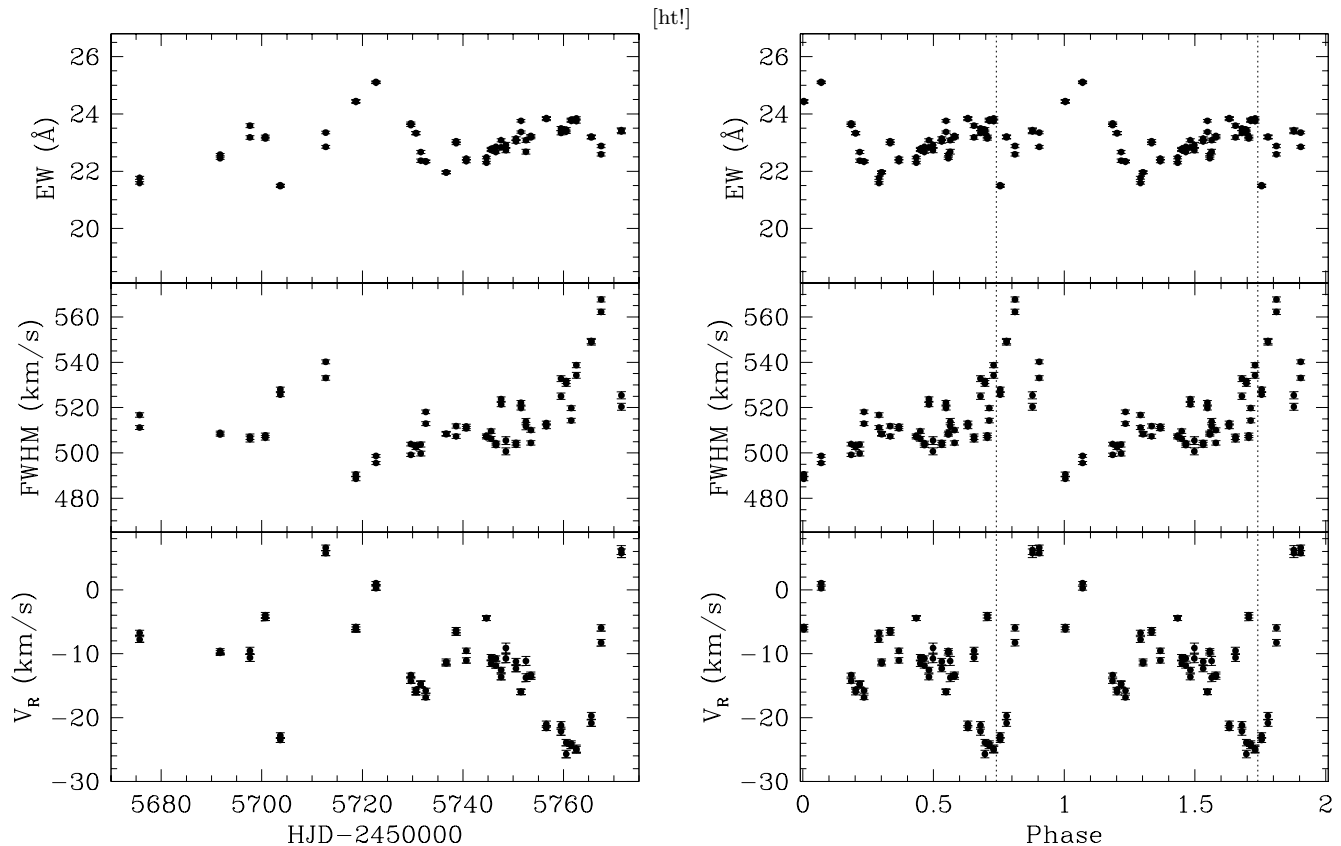


Figure 2. Left: time evolution of the $H\alpha$ line parameters in MWC 656. Both the $FWHM$ and centroid velocities show significant variability with maxima roughly separated by ~ 60 d. Right: Same but folded on the 60.37 d period of Williams et al. (2010). Phase 0 has been set to the time of maximum optical brightness at HJD 2453243.3. The vertical dotted line denotes the phase of the periastron (see text).

Table 3. Orbital solution for MWC 656 and MWC 148.

Parameter	MWC 656	MWC 148
P_{orb} (days)	60.37 (fixed)	321 (fixed)
T_0 (HJD-2,450,000)	3243.3 (fixed)	4857.5 (fixed)
e	0.4 (fixed)	0.83 \pm 0.08
ω (deg)	71 \pm 23	129 \pm 17
γ (km s $^{-1}$)	-2.8 \pm 9.4	48.3 \pm 8.9
ϕ_{peri}	0.74 \pm 0.05	0.967 \pm 0.008
K_{opt} (km s $^{-1}$)	41.7 \pm 6.8	22.0 \pm 5.7
$a_1 \sin i$ (R_{\odot})	45.6 \pm 7.3	77.6 \pm 25.9
$f(M)$ (M_{\odot})	0.35 $^{+0.20}_{-0.15}$	0.06 $^{+0.15}_{-0.05}$
σ (km s $^{-1}$)	20.3	12.8

tests using several orbital configurations indicate that an uncertainty of ± 0.1 for $e = 0.4$ is appropriate. Note that we have masked the one discrepant point at phase 0 from the fit. A close look to this spectrum shows a flatter He I 4471 Å profile than the rest, possibly due to disc emission. In any case, this point has a marginal impact in the final solution since it slightly reduces the eccentricity to 0.35 while the remaining orbital parameters are virtually unaffected. Table 3 presents our final best-fitting parameters.

5 ANALYSIS OF MWC 148

In this section we repeat the previous analysis for the star MWC 148. The left panel in Figure 4 presents the behaviour of the main $H\alpha$ parameters over our baseline of nearly three years. The LT data reveal a smooth sinusoidal modulation in all three parameters with a timescale which, at first glance, seems consistent with the 321 d X-ray period of Bongiorno et al. (2011). This is better depicted in the right panel of Figure 4, where the $H\alpha$ parameters are folded on the 321 d period. The plot also shows that the EW s of the MT and, in particular, the ST spectra are systematically lower than the rest. For comparison, Aragona et al. (2010) report $EW=52.3$ Å on JD 2454757–92. The $FWHM$ and centroid velocities are again consistently lower in the MT and ST spectra. A plot of the average $H\alpha$ profiles demonstrates that the line becomes weaker and narrower in the MT and ST spectra because of the gradual appearance of a broad absorption throat with a full-width-zero-intensity $FWZI \sim 2000$ km s $^{-1}$ (see bottom panel in Figure 5). This is characteristic of the faint states of Be stars which are likely related to episodes of reduced circumstellar envelope (Grundstrom & Gies 2006). Broad absorptions are also detected in $H\beta$ and the myriad of Fe II lines which plague the blue spectral range such as Fe II 4924 Å and 5018 Å (see top panel in Figure 5). These absorptions will likely contaminate most of the photospheric lines. Therefore, we decided

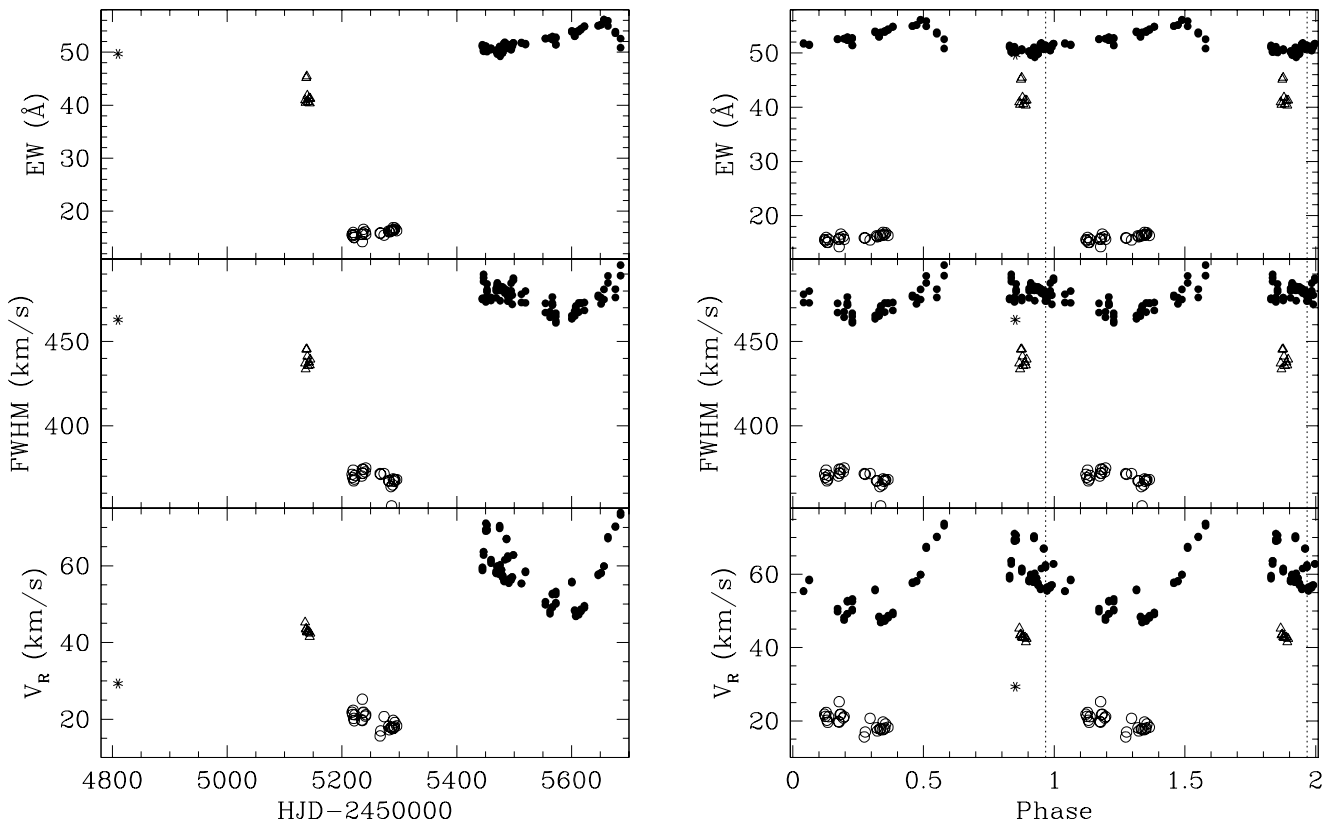


Figure 4. Left: time evolution of the $H\alpha$ line parameters in MWC 148. Different symbols indicate different datasets as follows: asterisk (WHT), open triangles (MT) open circles (ST) and filled circles (LT). Note the sinusoidal modulation in the LT data with a timescale of ≈ 300 d. Errorbars are not plotted because they are always smaller than the symbol size. Right: same as in the left panel but folded on the 321 d X-ray period of Bongiorno et al. (2011). Phase 0 has been set to HJD 2454857.5. Periastron is marked by a vertical dotted line (see text).

to exclude these spectra from the study of the radial velocity curve of the Be star.

As in MWC 656, radial velocities were obtained by cross-correlating every blue INT/WHT/LT spectrum with a template produced from the average of all. Prior to this, each spectrum was rebinned into a uniform velocity scale of 23 km s^{-1} per pixel. Cross-correlation was performed over spectral windows covering the He I lines 4471 Å, 4713 Å and 5048 Å. Additional regions containing lines of Si III (4568 & 4575 Å), C III/O II (4639–4650 Å) and He II 4686 Å were also included. These absorption features are stronger in MWC 148 than in MWC 656 because of its earlier spectral type. The rest velocity of the template was again determined through a Gaussian fit to the core of the He I 4471 Å line and it was subsequently added to the cross-correlation velocities. The radial velocity curve, folded on the 321 d period is displayed in Figure 6. In spite of the limited phase coverage and velocity scatter, a sharp velocity minimum is detected. The narrowness of this feature prompts for a large eccentricity. We have attempted to model this radial velocity curve with the SBOP fitting code, fixing the orbital period to 321 d. Following Bongiorno et al. (2011), we have defined phase 0 as HJD 2454857.5 which was arbitrarily set to the date of the first *Swift*/XRT observation in their paper. The best-fitting orbital elements are presented in the second column of Table 3.

6 DISCUSSION

In this paper we have presented an extensive spectroscopic database of MWC 656 and MWC 148, the optical counterparts of the candidate γ -ray binaries AGL J2241+4454 and HESS J0632+057 respectively. Our data show evidence for long-term modulation in the main $H\alpha$ parameters, consistent with the proposed orbital periods of 60.37 d and 321 d respectively. These modulations are likely produced by tidal instabilities in the circumstellar envelopes triggered by the motion of the compact star in an eccentric orbit. Circumstantial support for the orbital nature of the $H\alpha$ variability is given by the EW values. The EW of the $H\alpha$ line in Be/X-ray binaries provides a good estimate of the size of the circumstellar disc and, because this is truncated by the tidal torques of the compact star, a simple relation $EW(H\alpha) \propto P_{\text{orb}}^{4/3}$ is expected (Reig 2011). It should be noted that this correlation holds for the maximum EW observed over a long length of time. We measure $EW = 25 \text{ Å}$ for MWC 656 and 56 Å for MWC 148 which, according to the empirical $P_{\text{orb}} - EW(H\alpha)$ diagram in Fig.15 of Reig (2011), suggest $P_{\text{orb}} \approx 90$ and 250 d respectively. Given the scatter of the figure, these are fully consistent with the orbital periods proposed in the literature.

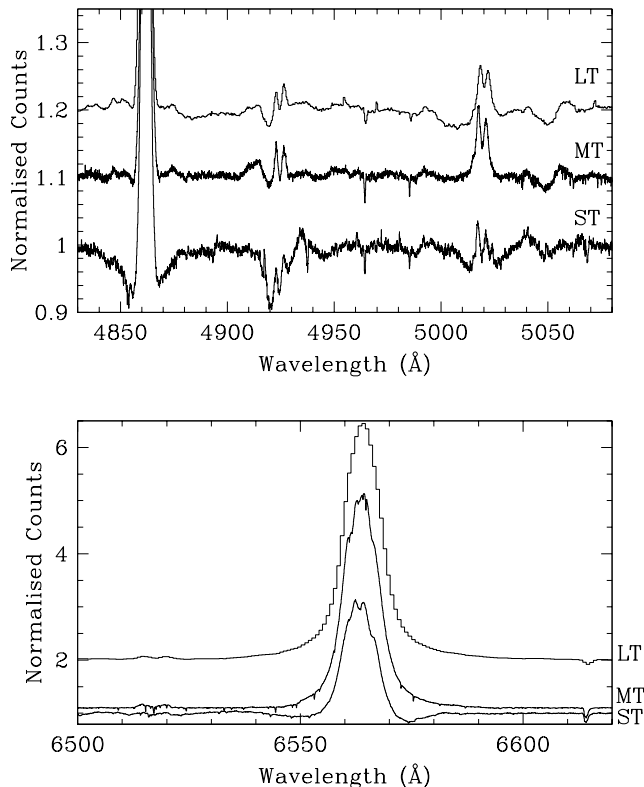


Figure 5. Average spectra of MWC 148 showing the evolution of several circumstellar disc profiles. The emission lines weaken because of the appearance of broad absorption throats, especially clear in the ST spectra.

6.1 Masses of the compact stars

Further, we have detected radial velocity variations in the photospheric lines of both MWC 656 and MWC 148. Assuming that their orbital periods are 60.37 d and 321 d, we produce phase folded radial velocity curves which allow us to constrain their orbital elements for the first time. In particular, we determine the mass function of the compact object to be $f(M) = M_c^3 \sin^3 i / (M_c + M_{\text{opt}})^2 = 0.35_{-0.15}^{+0.20} M_{\odot}$ for MWC 656 and $0.06_{-0.05}^{+0.15} M_{\odot}$ for MWC 14. In this equation, M_c and M_{opt} stand for the masses of the compact and the optical star respectively. Unfortunately, no pulsations have been detected from the compact stars yet and hence we cannot provide a full solution to the stellar masses and the nature of the invisible companions at this point. However, some speculations can be made based on our determination of the rotational broadenings $v \sin i$.

We measure $v \sin i \sim 346 \text{ km s}^{-1}$ for MWC 656 and $\sim 373 \text{ km s}^{-1}$ for MWC 148. A lower limit to the inclination can be derived from the condition that the optical companion should not exceed 0.9 times the critical rotational velocity v_{crit} . According to Table 2 in Yudin (2001), $v_{\text{crit}} \sim 565 \text{ km s}^{-1}$ for a B0 V which implies $i \gtrsim 47^\circ$ for MWC 148. On the other hand, $v_{\text{crit}} \sim 420 \text{ km s}^{-1}$ for a B3 IV and hence $i \gtrsim 66^\circ$ for MWC 656. These estimates obviously assume that the Be star’s spin axis and the orbital axis are aligned, which may not be true considering a

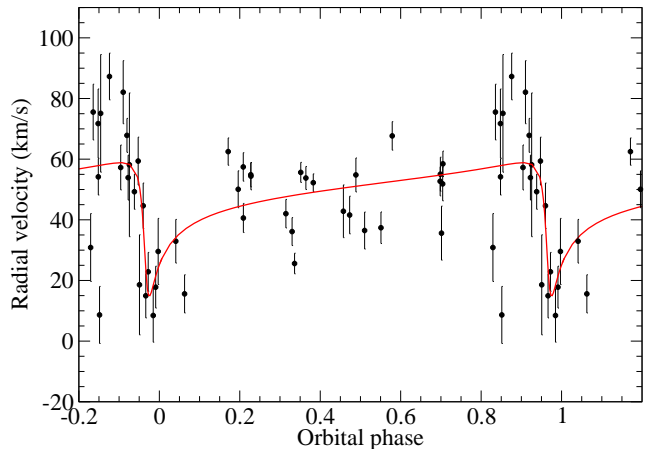


Figure 6. Radial velocity curve of MWC 148 folded on the 321 d period. The best eccentric orbital solution is overplotted. Phase 0 is set to HJD 2454857.5.

possible kick during the supernova explosion that forms the compact object.

In addition, the presence of double peaked emission profiles in our spectra also hints for a moderately high inclination. In particular, the Fe II lines are optically thin and their profiles reflect the Keplerian rotation in the emitting part of the Be disc (Hanuschik 1996). Therefore, we can use their *FWZI* to estimate the binary inclination through $FWZI/2 \times \sin i = (GM_{\text{opt}}/R_{\text{opt}})^{1/2}$. We measure *FWZI* ($\lambda 5018$) $\sim 1300 \text{ km s}^{-1}$ in MWC 148 and, using $M_{\text{opt}} \simeq 13.2$ – $19.0 M_{\odot}$ and $R_{\text{opt}} \simeq 6.0$ – $9.6 R_{\odot}$ from Aragona et al. (2010), we find $i \sim 71$ – 90° . Regarding MWC 656 we measure *FWZI* ($\lambda 5018$) $\sim 1000 \text{ km s}^{-1}$ which, combined with $M_{\text{opt}} \simeq 5.8$ – $9.8 M_{\odot}$ and $R_{\text{opt}} \simeq 4.7$ – $8.5 R_{\odot}$ from Williams et al. (2010), yield $i \sim 70$ – 76° . These estimates, however, should be regarded as mere upper limits because the region where the Fe II lines are produced is unlikely to extend down to the surface of the Be star.

We also note that the Fe II profiles do not exhibit deep central absorptions below the continuum, characteristic of shell stars. Shell lines are thought to be produced by obscuration of the star by the circumstellar disc and are only observed at $i \geq 80^\circ$ (Hanuschik 1996), which sets a rough upper limit to the inclination in both MWC 148 and MWC 656. In summary, crude values of $i \simeq 47$ – 80° for MWC 148 and $i \simeq 67$ – 80° for MWC 656 seem the most plausible given the available constraints at this point. Bringing the constraints to the inclination and the Be stellar masses from Williams et al. (2010) and Aragona et al. (2010) into the mass function equation results in $M_c \simeq 2.7$ – $5.5 M_{\odot}$ for MWC 656 and 1.3 – $7.1 M_{\odot}$ for MWC 148, although these numbers should be treated with caution because of the large uncertainties involved in this calculation. First, the binary inclinations are loosely constrained and need to be refined. Further, our orbital solution is based on a limited data set which requires confirmation through a more extended baseline. In particular, observations of MWC 148 around the periastron at phase 0 are strongly encouraged. Unfortunately, the long orbital period coupled to the annual solar cycle means that the first opportunity for ground observations will not happen until March 2015.

The wide range of masses allowed by our orbital solu-

tions prevent us from deciding whether the compact objects in MWC 148 and MWC 656 are neutron stars or black holes. However, their long orbital periods place them among the widest γ -ray binaries, only after PSR B1259–63, and this offers an opportunity to probe the nature of the compact star through the detection of radio pulsations. Previous attempts in LS 5039 and LS I +61 303 have failed presumably due to strong free-free absorption by the dense stellar winds (see McSwain et al. 2011 and references therein). In principle, the detection of radio pulses might be possible in both MWC 148 and MWC 656 around apastron phases due to their wider orbits. X-ray pulses are also expected to arise through synchrotron emission in the magnetosphere of a rotationally-powered pulsar or from an accreting neutron star. Deep searches for X-ray pulsations have been performed in both LS 5039 and LS I +61 303 with null results (See Rea et al 2010, 2011 and included references). This implies than the putative pulsars are spinning faster than ~ 5.6 ms, the pulsar beam is pointing away from our line of sight or X-ray pulsations are restricted to a limited range of orbital phases. We note that Rea et al. (2010) could not either find pulsations in MWC 148 using *Chandra* data during one outburst nor in *XMM – Newton* data during quiescence. These observations had a time resolution of only 199.2 ms and, according to our ephemeris, were performed at orbital phases 0.33 and 0.46, respectively. Therefore, the *XMM – Newton* data coincide with the apastron passage, where Compton scattering is lower and hence more favorable for the detection of X-ray pulses. More higher time resolution observations of both MWC 656 and MWC 148 at different orbital phases are urgently required to test the nature of their compact stars.

6.2 Orbital variability

Aside from the stellar masses, our orbital solutions do provide interesting information on the geometry of the γ -ray binaries and properties of the observed X-ray/VHE radiation. Figure 7 presents the relative motion of the compact star around the optical companion for both MWC 656 and MWC 148 as seen from above i.e. $i = 0^\circ$. The figure was produced using the stellar masses and radii from Williams et al. (2010) and Aragona et al. (2010) and assuming a $1.4 M_\odot$ compact star. Our ephemeris imply that the X-ray outbursts in MWC 148 are delayed by ~ 100 d or 0.3 orbital phases with respect to the periastron passage. This is remarkably similar to LS I +61 303 where X-ray outbursts are observed ~ 0.2 orbital phases passed the closest approach of the stellar components (Casares et al. 2005a).

Regarding MWC 656, the maximum of the optical modulation takes place ~ 0.25 orbits after periastron. A similar phase shift of the photometric maximum is seen in LS I +61 303 (Mendelson & Mazeh 1989; Paredes et al. 1994). In addition, the right frame in Figure 2 shows that the *EW* of the $H\alpha$ line peaks ~ 0.3 orbital phases passed periastron. This behaviour seems consistent with an scenario where the modulation in both the continuum flux and the (optically thick) $H\alpha$ flux is caused by the visibility of a one-arm tidal wave in the circumstellar disc, triggered by the close passage of the neutron star. For instance, Okazaki et al. (2002) present SPH simulations of a Be/X-ray binary with $P_{\text{orb}}=24.3$ d and $e = 0.34$ which is not

too far from the parameters that we derive for MWC 656. Their simulations (see Figures 10 and 11 in the paper) show that a spiral density wave, excited by the periastron passage, is fully developed around phase ~ 0.25 past periastron. Furthermore, Williams et al. (2010) observed a rapid variability of the V/R ratio of the $H\gamma$ emission and suggested it could be associated with the changing tidal effects of the companion on the disk, which is specially strong near periastron. Indeed, these observations correspond to orbital phases 0.82 ± 0.02 and 0.84 ± 0.02 which according to our ephemeris are just ~ 0.08 and ~ 0.10 in phase after periastron. At phase ~ 0.8 we also observe a rapid transition of the $H\alpha$ centroid from negative to positive velocities, coincident with a peak in the *FWHM* (see right frame in Figure 2).

In view of the new orbital ephemeris of MWC 656 it is also interesting to put in context the multiwavelength observations of the source. First of all, the *AGILE* detection between 25 July 2010 at 01:00 UT and 26 July 2010 at 23:30 UT (Lucarelli et al. 2010), corresponding to an orbital phase range of 0.77–0.80, took place just after (or even during) periastron. A maximum of the GeV emission takes place during periastron in LS 5039 (Abdo et al. 2009a) and soon after it in LS I +61 303 (Abdo et al. 2009b). The fact that the *AGILE* flare in MWC 656 happens very close to the inferior conjunction of the compact object ($w = 71 \pm 23$ deg), coupled with its high orbital inclination, may explain the weak GeV emission through a reduction in the Compton scattering cross-section for large angles (Khanguyan et al. 2008). All these facts reinforce the association between the Be star MWC 656 and the gamma-ray source AGL J2241+4454 and, even with the lack of γ -ray detections aside from the flare seen by *AGILE* during a single periastron passage, give strong support to the idea that MWC 656 is a new γ -ray binary.

On the other hand, MWC 148 has only shown significant VHE radiation simultaneous to the X-ray flare episodes which occur ~ 0.3 phases past periastron. Indeed, according to our ephemeris, the *VERITAS* upper limits (Acciari et al. 2009) were obtained during the phase intervals 0.6–0.72, 0.86–0.93 and 0–0.01, corresponding to low levels of quiescent X-ray emission (Bongiorno et al. 2011). Conversely, the H.E.S.S. discovery observations occurred at phases 0.32 and 0.36–0.46, coincident with periods of X-ray flares. Further detections of MWC 148 at VHE during X-ray active phases have been reported by Ong et al. (2011) and Mariotti et al. (2011).

6.3 The class of γ -ray binaries

The family of γ -ray binaries is growing fast with the recent discovery of AGL J2241+4454, HESS J0632+057.1 and 1FGL J1018.6–5856. These add up to the group of "classic" γ -ray binaries PSR B1259–63, LS 5039 and LS I +61 303. Table 4 summarizes some of their main physical parameters. They all contain late O-Be stars with strong winds and stellar radii in the range ~ 7 – $10 R_\odot$. The table shows a possible correlation between the eccentricity and the orbital period and this is illustrated in figure 8. A least-squared linear fit yields:

$$e = 0.206(19) \times \log P_{\text{orb}} + 0.233(60) \quad (1)$$

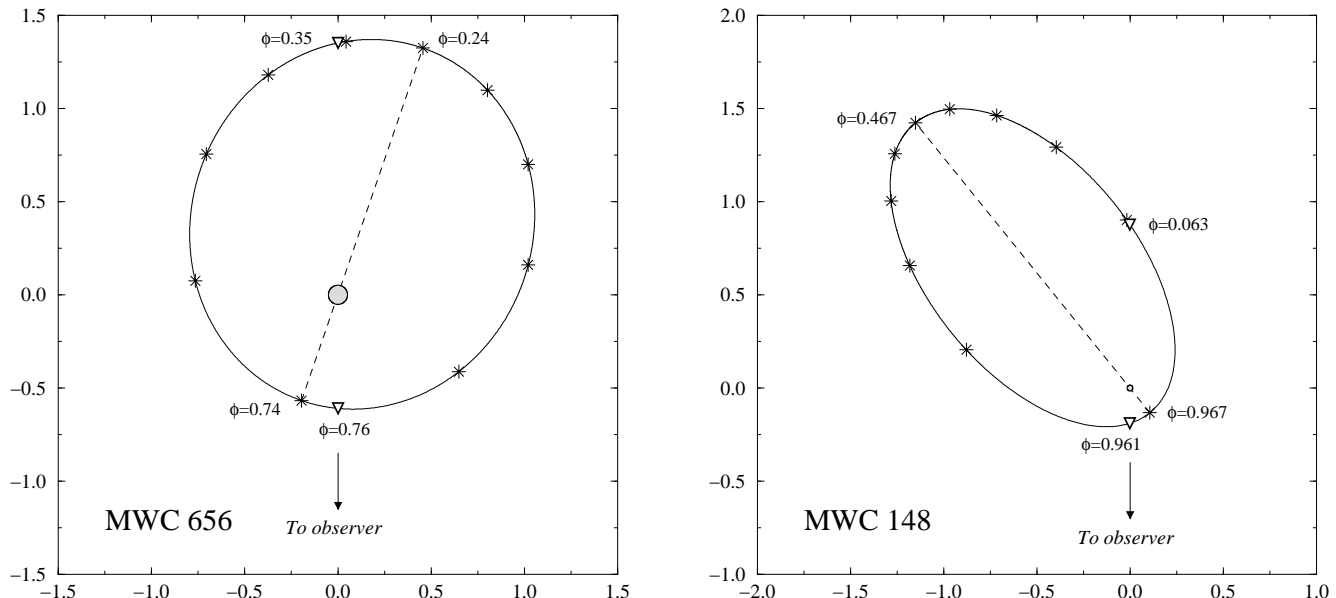


Figure 7. Left: relative orbit of the compact object around the optical star in MWC 656 as seen from above the orbital plane. Phases of periastron and apastron are indicated and joined by a dashed line which depicts the major axis of the orbit. Stars mark 0.1-phase intervals from periastron whereas open triangles indicate the phases of the inferior conjunction and superior conjunction of the compact star. The coordinates are in units of the orbital semimajor axis. Right: same for MWC 148. Note that the semimajor axis is 0.64 AU in MWC 656 and 2.38 AU in MWC 148

For comparison, Figure 8 also presents 35 high-mass X-ray binaries (HMXBs) with X-ray pulsars from Liu et al. (2006) and Martin et al. (2009). HMXBs tend to lie below the linear regression of γ -ray binaries, i.e. for a given orbital period they have lower eccentricities. The only exceptions are 4U 1850–03, 0535–668 and the SMC binary J0045–7319, all with $e > 0.8$. In particular, the latter two have $P_{\text{spin}} < 1$ s and hence a high spin-down power which makes them potential candidates for γ -ray emission.

The reason behind the $P_{\text{orb}} - e$ correlation in γ -ray binaries stems from the fact that small stellar separations are required to trigger VHE radiation and this can only happen for long orbital periods if the eccentricity is large. Conversely, for short orbital periods high eccentricities would imply that the compact object passes through the stellar atmosphere of the companion, clearly an unstable situation. The separation of the two stars at periastron $a(1 - e)$ and apastron $a(1 + e)$ is also listed in Table 4, assuming that the compact star is a $1.4 M_{\odot}$ neutron star. As expected, the most compact binaries LS 5039, 1FGL J1018.6–5856 and LS I +61 303 show persistent VHE and/or HE radiation modulated with their orbital periods whereas only transient radiation is detected in PSR B1259–63 around periastron. This seems to imply that stellar separations $\lesssim 1$ a.u. or $\lesssim 25 R_{\text{opt}}$ are required for the efficient production and modulation of the HE/VHE radiation but the picture is certainly more complex. For instance, MWC 656 has been detected up to GeV energies only once during a flare episode at periastron whereas MWC 148 is regularly detected at TeV ~ 0.3 orbital phases past periastron. Aside from sensitivity limitations of different satellite/telescopes, other processes such as photon-photon annihilation and the subsequent production of electron-positron pairs are likely responsible for the wide phenomenology observed. In particular, the binary inclina-

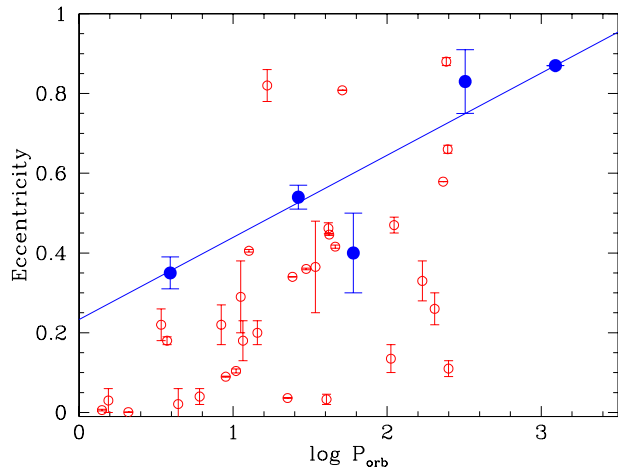


Figure 8. Eccentricity versus orbital period for γ -ray binaries (filled circles) and high mass X-ray binaries from the catalogue of Liu et al. 2007 (open circles). A linear fit to the γ -ray binaries is overplotted.

tion and argument of periastron are important parameters for the attenuation of the VHE radiation and modelling the observed amplitudes (Dubus 2006).

It is well established that accretion discs in Be/X-ray binaries are truncated by the tidal torque of the neutron star (Negueruela & Okazaki 2001). Since the EW of the $H\alpha$ emission is a good proxy of the disc size this results in the well known correlation between P_{orb} and the maximum observed $EW(H\alpha)$ (Reig et al. 1997; Reig 2011). Most γ -ray binaries contain Be primaries and it is interesting to test whether a similar correlation holds. Table 4 lists the range of $EW(H\alpha)$ values reported in literature for the γ -

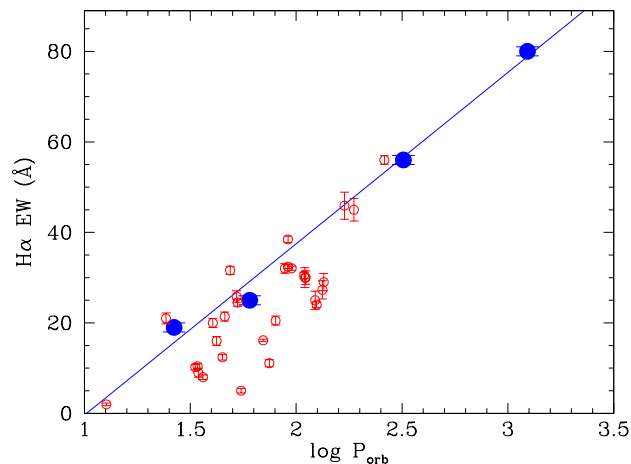


Figure 9. Maximum EW of the $H\alpha$ emission line versus orbital period for γ -ray binaries (filled circles) and Be/X-ray binaries (open circles). The latter include Milky Way and SMC binaries from Reig (2011). A linear fit to the γ -ray binaries is overplotted. Note that LS 5039 is not included because the primary is not a Be star.

ray binaries. Significant long-term and orbital variability is typically seen in Be/X-ray binaries and the same is observed in the γ -ray binaries. In this paper we detect a maximum EW for MWC 656 at ~ 0.3 phases past periastron, in agreement with what is observed in LS I +61 303 (McSwain et al. 2010). On the other hand, the maximum EW for MWC 148 occurs at periastron. In any case, only the maximum EW values are driven by the disc truncation radius. Figure 9 plots the maximum $EW(H\alpha)$ measured in γ -ray binaries with Be primaries versus P_{orb} and we note that they follow the linear regression:

$$EW = 37.8(5.0) \times \log P_{orb} - 38.3(11.4) \quad (2)$$

For comparison, Figure 9 also shows EW s of Be/X-ray binaries from Reig (2011). As in the case of the eccentricity, we observe that γ -ray binaries define the higher envelope of the distribution i.e. for a given orbital period Be/X-ray binaries tend to have smaller decretion discs than γ -ray binaries. This is somehow surprising in a millisecond pulsar scenario because it implies that the relativistic pulsar wind does not "erode" significantly the circumstellar disc even during periastron passage. However, it is also true that, given the large eccentricities of γ -ray binaries, they only spend a short fraction of time close to the Be star, perhaps preventing efficient truncation. Interestingly, equations 1 and 2 provide a new tool for a rough estimate of two fundamental parameters (such as P_{orb} and e) in Be/ γ -ray binaries simply from the EW of the $H\alpha$ emission. This can be tested with future observations of newly discovered γ -ray binaries.

7 SUMMARY

We have reported optical spectroscopy of MWC 656 and MWC 148, the optical counterparts of the γ -ray sources AGL J2241+4454 and HESS J0632+057 respectively. Our data show that the main $H\alpha$ parameters are modulated with the 60.37 d optical photometric period in MWC 656 and

with the 321 d X-ray period in MWC 148. This is likely produced by the visibility of a tidal wave in the Be disc, triggered by the close passage of a compact star. In addition, we present radial velocity curves for the two stars and the first constraints to the binary parameters. Both stars display similarities with LS I +61 303, where photometric maxima and X-ray outburst are delayed by ~ 0.3 phases past periastron. When compared to other γ -ray binaries, we find that the eccentricity is correlated with the orbital period. This is explained by the small stellar separations needed for triggering the γ -ray activity. The maximum EW of the $H\alpha$ emission is also correlated with orbital period. This is reminiscent of Be/X-ray binaries and suggest that the size of circumstellar discs in γ -ray binaries is tidally truncated by the compact companion.

8 ACKNOWLEDGMENTS

We thank D. Steeghs and L. van Spaandonk for kindly taking the WHT spectra. We are also grateful to E. Grundstrom for sharing her EW measurements of PSR B1259-63 with us and to P. Reig for the EW data of Be X-ray binaries. Based on observations made with the INT and WHT operated on the island of La Palma by the Isaac Newton Group in the Spanish Observatorio del Roque de Los Muchachos of the Instituto de Astrofísica de Canarias (IAC). The Liverpool Telescope is operated on the island of La Palma by Liverpool John Moores University in the Spanish Observatorio del Roque de los Muchachos of the Instituto de Astrofísica de Canarias with financial support from the UK Science and Technology Facilities Council. Also based on observations made with the Mercator operated on the island of La Palma by the Univ. of Leuven and the Obs. of Geneva in the Spanish Observatorio del Roque de Los Muchachos of the IAC. This research has been supported by the Spanish Ministerio de Ciencia e Innovación (MICINN) under grants AYA2010-18080, AYA2010-21782-C03-01, AYA2010-21697-C05-05 and FPA2010-22056-C06-02. M.R. acknowledges financial support from MICINN and European Social Funds through a *Ramón y Cajal* fellowship. J.M.P. acknowledges financial support from ICREA Academia. Partly funded by the Spanish MEC under the Consolider-Ingenio 2010 Program grant CSD2006-00070: "First science with the GTC" (<http://www.iac.es/consolider-ingenio-gtc/>). MOLLY software developed by T. R. Marsh is gratefully acknowledged.

REFERENCES

- Abt H.A., Levato H., Grosso M., 2002, ApJ, 573, 359
- Abdo, A. A., Ackermann, M., Ajello, M., et al., 2009a, ApJ, 706, L56
- Abdo, A. A., Ackermann, M., Ajello, M., et al., 2009b, ApJ, 701, L123
- Acciari, V. A., et al., 2009, ApJ, 698, L97
- Aharonian F.A. et al., 2007, A&A, 469, L1
- Aragona C. et al., 2009, ApJ, 698, 514
- Aragona C., McSwain M.V., De Becker M., 2010, ApJ, 724, 306
- Bongiorno S.D. et al., 2011, ApJ, 737, L11

Table 4. The family of γ -ray Binaries sorted by orbital period

Name	γ -ray Activity	Spectral Type	M_{opt} (M_{\odot})	R_{opt} (R_{\odot})	i (deg)	P_{orb} (days)	e	$a(1-e)$ (AU)	$a(1+e)$ (AU)	EW (\AA)	d (kpc)	Reference ^a
LS 5039	HE, VHE	O6.5 V((f))	20–26	9–10	13–64	3.91	0.35	0.09	0.19	–2.8	2.5	(1)
1FGL J1018.6–5856	HE	O6 V((f))	~37	~10	–	16.58	–	–	–	–	~5.4	(2), (3)
LS I +61 303	HE, VHE	B0 Ve	10–15	~7	10–60	26.50	0.54	0.19	0.64	8–19	1.9	(4), (5), (6), (7)
MWC 656	HE	B3 IVne+sh	6–10	5–9	67–80	60.37	0.40	0.38	0.89	19–25	~2.6	(8), this paper
MWC 148	VHE	B0 Vpe	13–19	6–10	47–80	321	0.83	0.40	4.35	48–56	~1.4	(9), this paper
PSR B1259–63	HE, VHE	O9.5 Ve	31	9	19–31	1236.79	0.87	0.93	13.44	40–80	2.3	(10), (11), (12)

^a (1) Casares et al. 2005b. (2) Corbet et al. 2011. (3) Napoli et al. 2011. (4) Aragona et al. 2009. (5) Zamanov et al. 1999. (6) Casares et al. 2005a. (7) McSwain et al. 2010. (8) Williams et al. 2010. (9) Aragona et al. 2010. (10) Negueruela et al. 2011. (11) Johnston et al. 1994. (12) Grundstrom et al., private communication

Dhawan V., Mioduszewski A., Rupen M., 2006, PoS, Proceedings of the VI Microquasar Workshop: Microquasars and Beyond, ed. T. Belloni, 52.1
 Dubus G., 2006, A&A, 451, 9
 Casares J., Ribas I., Paredes J.M., Martí J., Allende Prieto C., 2005a, MNRAS, 360, 1105
 Casares J., Ribó M., Ribas I., Paredes J.M., Martí J., Herrero A., 2005b, MNRAS, 364, 899
 Casares J. et al., 2011, in "High-Energy Emission from Pulsars and their Systems", Astrophysics and Space Science Proceedings, ed. N. Rea and D.F. Torres, Springer-Verlag, p. 559
 Corbet R.H.D. et al., 2011, ATel, 3221
 Etzel, P. B., 1985, "SBOP - Spectroscopic Binary Orbit Program", Program's Manual
 Falcone A.D. et al., 2010, ApJ, 708, L52
 Finger M.H. et al., 1999, ApJ, 517, 449
 Gray D.F., 1992, The Observation and Analysis of Stellar Photospheres. CUP, Cambridge
 Gutiérrez-Soto J., Fabregat J, Suso J., Lanzara M., Garrido R., Hubert A.-M., Floquet M., 2007, A&A, 476, 927
 Grundstrom E.D., Gies D.R., 2006, ApJ, 651, L53
 Hanuschik R.W., Hummel W., Sutorius E., Dietle O., Thimm G., 1996, A&AS, 116, 309
 Hinton J.A., Hofmann W., 2009, ARA&A, 47, 523
 Hinton J.A. et al., 2009, ApJ, 690, L101
 Horne K., 1986, PASP, 98, 609
 Johnston S., Manchester R.N., Lyne A.G., Nicastro L., Spyromilio J., 1994, MNRAS, 268, 430
 Khangulyan D., Aharonian F., Bosch-Ramon V., 2008, MNRAS, 383, 467
 Liu Q.Z., van Paradijs J., van den Heuvel E.P.J., 2006, A&A, 455, 1165
 Lucarelli F. et al., 2010, ATel, 2761
 Mariotti, M., et al., 2011, ATel, 3161
 Marsh T.R., Robinson E.L., Wood J.H., 1994, MNRAS, 266, 137
 Martin R.G., Tout C.A., Pringle J.E., 2009, MNRAS, 397, 1563
 McSwain M.V., Grundstrom E.D., Gies D.R., Ray P.S., 2010, ApJ, 724, 379
 McSwain M.V., Ray P.S., Ransom S.M., Roberts M.S.E., Dougherty S.M., Pooley G.G., 2011, ApJ, 738, 105
 Mendelson, H., & Mazeh, T., 1989, MNRAS, 239, 733
 Moldón J., Johnston S., Ribó M., Paredes J.M., Deller

A.T., 2011b, ApJ, 732, L10
 Moldón J., Ribó M., Paredes J.M., 2011a, A&A, 533, L7
 Napoli, V.J., McSwain M.V., Boyer A.N.M., Roettenbacher R.M., 2011, PASP, 123, 1262
 Negueruela, I., Okazaki A.T., 2001, A&A, 369, 108
 Negueruela, I., Ribó M., Herrero A., Lorenzo J., Khangulyan D., Aharonian F.A., 2011, ApJ, 732, L11
 Ong, R., et al., 2011, ATel, 3153
 Okazaki A.T., Bate M.R., Ogilvie G.I., Pringle J.E., 2002, MNRAS, 337, 967
 Paredes, J. M., Marziani, P., Martí, J., et al. 1994, A&A, 288, 519
 Paredes J.M., 2011, Il Nuovo Cimento C - Colloquia on physics, arXiv1101.4843
 Porter J.M., Rivinius Th., 2003, PASP, 115, 1153
 Rea N., Torres D.F., van der Klis M., Jonker P.G., Méndez M., Sierpowska-Bartosik A., 2010, MNRAS, 405, 2206
 Rea N., Torres D.F., 2011, ApJ, 737, L12
 Rea N. et al., 2011, MNRAS, 416, 1514
 Reig P., Fabregat J, Coe M.J., 1997, A&A, 322, 193
 Reig P., 2011, Ap&SS, 332, 1
 Ribó M., Paredes J.M., Moldón J., Martí J., Massi M., 2008, A&A, 481, 17
 Skilton J.L. et al., 2009, MNRAS, 399, 317
 Townsend R.H.D., Owocki S.P., Ud-Doula A., 2007, MNRAS, 382, 139
 Williams S.J. et al., 2010, ApJ, 723, L93
 Yudin R.V., 2001, A&A, 368, 912
 Zamanov R.K., Martí J., Paredes J.M., Fabregat J., Ribó M., Tarasov A.E., 1999, A&A, 351, 543